Polymer 51 (2010) 2021–2032

Contents lists available at ScienceDirect

Polymer

journal homepage: www.elsevier.com/locate/polymer

Synthesis, characterization, and bulk crosslinking of polybutadiene-*block*-poly(2-vinyl pyridine)-*block*-poly(*tert*-butyl methacrylate) block terpolymers

Felix Schacher [a,1,*], Jiayin Yuan [a,2], Heiko G. Schoberth [b], Axel H.E. Müller [a,*]

[a] *Makromolekulare Chemie II and Bayreuther Zentrum für Kolloide und Grenzflächen, Universität Bayreuth, D-95440 Bayreuth, Germany*
[b] *Physikalische Chemie II, Universität Bayreuth, D-95440 Bayreuth, Germany*

ARTICLE INFO

Article history:
Received 4 November 2009
Received in revised form
24 February 2010
Accepted 26 February 2010
Available online 4 March 2010

Keywords:
Polymeric nanoparticles
Block terpolymers
Anionic polymerization

ABSTRACT

We report on the synthesis and characterization of triblock terpolymers, polybutadiene-*block*-poly(2-vinyl pyridine)-*block*-poly(*tert*-butyl methacrylate) (PB-*b*-P2VP-*b*-P*t*BMA; BVT), via sequential living anionic polymerization in THF at low temperatures using *sec*-butyl lithium as initiator. In this work, 18 different BVT terpolymers were produced with volume fractions $\Phi_B : \Phi_V : \Phi_T$ in the range of 1 : 0.4…1.2 : 0.2…4.6. All polymers exhibit a very narrow molecular weight distribution (PDI < 1.1). They were characterized in terms of bulk morphology using small-angle X-ray scattering and transmission electron microscopy, unveiling mostly lamellar patterns or hexagonally arranged cylindrical structures. Some polymers displayed a partial gyroid structure coexisting with lamellar parts or cylinders with a non-continuous shell around the PB core and could serve as an interesting template for the facile generation of multi-compartmental self-assembled structures. In one case the middle block, P2VP, is forming a helix around the PB core. Crosslinking of the polybutadiene compartment of the bulk morphologies with an UV-photoinitiator was performed, followed by sonication-assisted dissolution of the aggregates to elucidate further use of the terpolymers for the generation of soft polymeric nanoparticles with controlled functionality. In that way, core-crosslinked cylindrical micelles could be generated and characterized.

1. Introduction

Block copolymers are an interesting and versatile class of materials and their tailor-made properties, in particular thin-film and bulk morphology, render them suitable for the demand of smaller and smaller feature sizes in nanotechnology [1]. Characteristic dimensions for the domain spacing of such micro-phase separated systems are in the range of 10–100 nm and the generation of nanostructured assemblies with different chemical properties raises opportunities for applications in the fields of catalysis, membrane research, molecular templating or drug delivery [2,3]. The peculiar advantage of block copolymers are their intrinsic dimensions, the ease of synthesis and the facile control over architecture and chemical functionality, turning them into manageable nanoscale tools [4–7]. In general, there are two possible ways for the use of block copolymer templates: either as prepared or after the selective removal of one component through a chemical process like etching or photodegradation [8,9].

To provide sufficient control over domain spacing and topology, well-defined block copolymers are required. Usually, this is achieved by a variety of controlled/"living" polymerization methods, among them typically are anionic/cationic polymerization, atom transfer radical polymerization (ATRP), reversible addition-fragmentation polymerization (RAFT) and group transfer polymerization (GTP). Once obtained, block copolymers self-assemble into a large variety of morphologies, depending on composition, architecture, block sequence and molecular weight [10]. As compared to AB diblock copolymers, considerably less work has been carried out on the synthesis and bulk properties of ABC block terpolymers [11]. Here, the resulting micro-phase separated structures are governed by several independent composition variables: the volume fractions (Φ_A, Φ_B), the three interaction parameters (χ_{AB}, χ_{BC}, χ_{AC}), the respective interfacial tensions (γ_{AB}, γ_{BC}, γ_{AC}) and previously mentioned factors like the chain topology [12–15]. Stadler et al. studied the phase behavior of polystyrene-*block*-polybutadiene-*block*-poly(methyl methacrylate) (SBM) block terpolymers and

* Corresponding authors. Tel.: +49 921 55 3399; fax: +49 921 55 3393.
E-mail addresses: axel.mueller@uni-bayreuth.de, felix.schacher@bristol.ac.uk (F. Schacher).
[1] Present address: School of Chemistry, University of Bristol, Cantocks Close, Bristol BS81TS, UK.
[2] Present address: MPI of Colloids and Interfaces, Department of Colloid Chemistry, D-14424 Potsdam, Germany.

0032-3861/$ – see front matter © 2010 Elsevier Ltd. All rights reserved.
doi:10.1016/j.polymer.2010.02.046

among the classical morphologies obtained for ABC type terpolymers like lamellae, core-shell cylinders and core-shell spheres they also reported on more complex micro-phase separated structures featuring helical assemblies [16], "knitting pattern" morphologies [17], and a new structural motif where two different cylindrical domains are formed instead of core-shell cylinders [18]. In our group, the self-assembly of polystyrene-*block*-polybutadiene-*block*-poly(*tert*-butyl methacrylate) (SBT) and SBM block terpolymers has been used to generate Janus structures, i.e. soft particles with two chemically different sides [19–22]. Further, polystyrene-*block*-poly(2-vinyl pyridine)-*block*-poly(*tert*-butyl methacrylate) (SVT) block terpolymers have been synthesized and studied intensively in the bulk [22] and in thin films on different substrates [23–25], the latter in particular with respect to the use of such systems as precursors for the fabrication of composite membranes.

The aim of this work is the synthesis and characterization of polybutadiene-*block*-poly(2-vinyl pyridine)-*block*-poly(*tert*-butyl methacrylate) (BVT) block terpolymers with different ratios of the block segments. The exchange of the rigid PS block against a soft PB segment compared to the SVT systems in combination with the high incompatibility between PB and P2VP [26] could provide a basis for different morphologies or functionalities. Well-defined terpolymers were obtained through sequential living anionic polymerization in THF at low temperatures using *sec*-butyl lithium as initiator. Different series of BVT terpolymers were produced with volume fractions $\Phi_A : \Phi_B : \Phi_C$ in the range of 1 : 0.4…1.2 : 0.2…4.6. All polymers exhibit a very narrow molecular weight distribution (below 1.1). Microphase separation of the BVT terpolymers was investigated in solution using small-angle X-ray scattering (SAXS) in THF above the order–disorder transition concentration and in the bulk via transmission electron microscopy (TEM). Phase allocation in the latter is accomplished through selective staining of either polybutadiene with OsO_4 [27] or poly(2-vinyl pyridine) with iodine [14]. The strongest incompatibility here is between the first block, polybutadiene, and the second block, poly(2-vinyl pyridine) ($\chi_{BV} = 0.325$) [26]. Reported values for the other compartments are $\chi_{VT} = 0.13$-0-26 and $\chi_{BT} = 0.007$ [28,29].

The polybutadiene compartment of the presented terpolymers is susceptible to crosslinking reactions. Fixation of the polymer morphologies after self-assembly was achieved through UV-light induced photo-polymerization of the cast polymer films after the incorporation of a suitable photoinitiator during the film casting process.

The nomenclature used throughout this manuscript is $B_aV_bT_c^x$, where *a*, *b*, and *c* are the weight fractions of the corresponding blocks and *x* is the overall molecular weight in kg/mol.

2. Experimental

2.1. Materials

Sec-butyllithium (Acros) was used without further purification. Butadiene (Messer-Griesheim) was passed through columns filled with molecular sieves (4 Å) and basic aluminum oxide. Afterwards it was condensed into a glass reactor and stored over dibutylmagnesium. 2-Vinyl pyridine (Fluka) was degassed and stirred with CaH_2 over night. The monomer was condensed on a high vacuum line into a round bottom flask containing 2 ml of triethylaluminum (solution in hexane, Aldrich) per 10 ml 2-vinylpyridine. The resulting yellow solution was stirred for 2 h. Subsequently, the calculated amount of monomer was condensed into a previously weighed glass ampoule and stored in liquid nitrogen until use. *Tert*-butyl methacrylate (BASF) was first degassed by 3 freeze–thaw cycles on a high vacuum line. Then tri-*n*-octylaluminum (solution in hexane, Aldrich) was added until a slight yellow colour of the resulting mixture persisted. The solution was stirred for 1 h and the calculated amount of monomer was condensed into a previously weighed glass ampoule and stored in liquid nitrogen until use. THF (Fluka) was distilled from CaH_2 and Na/K alloy. 1,1-diphenylethylene was distilled from sec-butyl lithium under reduced pressure.

2.2. Synthesis

The linear BVT block terpolymers were synthesized via sequential living anionic polymerizations of butadiene, 2-vinylpyridine and *tert*-butyl methacrylate in THF at low temperatures using *sec*-butyl lithium as initiator [30]. All polymerizations took place in the presence of alkoxides ($c = 0.013$ mol/L, typically this corresponds to a roughly 20-fold excess compared to the concentration of growing polymer chains). In a typical polymerization, 1,3-butadiene (30 mL, 18 g, 0.333 mol) was initiated at −70 °C with *sec*-BuLi (0.3 mL, 0.42 mmol) in THF (1500 mL) and polymerized for 5 h at −10 °C. Subsequently, 2-vinyl pyridine (17.3 mL, 16.3 g, 0.155 mol) was added to the stirred tank reactor via an ampoule. After polymerization of the second block (1 h), the living polybutadiene-*block*-poly(2-vinylpyridine) chain ends were endcapped with 1,1-diphenylethylene (DPE) in order to attenuate the nucleophilicity of the propagating species for 1 h at −50 °C. In that way, transfer reactions upon addition of the third monomer, *t*BMA (92 mL, 88.2 g, 0.62 mol), due to too high nucleophilicity could be suppressed [22,31]. During the polymerizations of the P*t*BMA block, samples were taken after different reaction times and precipitated into degassed isopropanol. Therefore we could obtain several series of BVT block terpolymers with a constant ratio of first to second block and increasing P*t*BMA content. Overall, in this work we synthesized 18 polymers with volume fractions $\Phi_B : \Phi_V : \Phi_T$ in the range of 1 : 0.4–1.2 : 0.2–4.6.

2.3. Crosslinking

Films of block terpolymers which showed suitable bulk morphologies, $B_{18}V_8T_{74}^{133}$ and $B_{14}V_{18}T_{68}^{165}$, were cast with additional photoinitiator, Lucirin-TPO© in this case. Typical, 1–10% photoinitiator with respect to the amount of PB (weight) was used. After fixation of the self-assembled structures, these were subjected to sonication procedures. In this way, multi-compartmental polymeric nanoparticles could be prepared on a gram scale. Within the scope of this work, no effect of the crosslinking procedure on the bulk morphologies was observed for different amounts of crosslinking agent in the range of 1–10 wt.%.

Crosslinking of the as-cast and annealed polymer films was carried out with a UV-lamp for 2 h (Hoehnle VG UVAHAND 250 GS, cut-off at 300 nm wavelength to avoid the depolymerization of the methacrylic compartment).

2.4. Structural characterization

For the structural characterization films of the BVT terpolymers were cast from THF by slow evaporation of the solvent over several days. The films were afterwards dried under vacuum at room temperature first for 24 h and at 50 °C for another 24 h. Subsequent annealing at elevated temperatures above the glass transition of all three blocks (130 °C) under vacuum did not lead to any change in the microdomain structure (the samples with high polybutadiene content started to decompose). For scattering experiments in solution the polymers were dissolved at concentrations above the order–disorder transition concentration in THF over several days. Typically, the order–disorder transition concentration (ODT) was in the range of 26–30 wt.% polymer.

Table 1
Block terpolymer characteristics.

Polymer[a]	PDI[b]	Volume fractions[c] $\Phi_B : \Phi_V : \Phi_T$	Bulk morphology[d]	Long period, TEM [nm][e]	Long period, SAXS, [nm][f]
$B_{47}V_{19}T_{34}^{61}$ (1)[g]	1.09	1 : 0.4 : 0.7	LL	70 ± 7	43 ± 2
$B_{38}V_{16}T_{46}^{82}$ (1)	1.09	1 : 0.4 : 1.1	LL	75 ± 7	57 ± 3
$B_{29}V_{12}T_{59}^{86}$ (1)	1.08	1 : 0.4 : 1.9	LL	68 ± 7	60 ± 3
$B_{22}V_9T_{69}^{109}$ (1)	1.08	1 : 0.4 : 2.9	CYL	55 ± 6	65 ± 3
$B_{18}V_8T_{74}^{133}$ (1)	1.08	1 : 0.4 : 3.9	CYL[h]	55 ± 6	67 ± 3
$B_{55}V_{26}T_{19}^{77}$ (2)	1.04	1 : 0.4 : 0.3	CYL	50 ± 5	n.d.
$B_{44}V_{20}T_{36}^{98}$ (2)	1.04	1 : 0.4 : 0.8	LL/GYR	45 ± 5/55 ± 6	74 ± 4/106 ± 5
$B_{38}V_{18}T_{44}^{112}$ (2)	1.03	1 : 0.4 : 1.1	LL	70 ± 7	50 ± 3
$B_{37}V_{17}T_{46}^{117}$ (2)	1.03	1 : 0.4 : 1.2	LL	70 ± 7	55 ± 3
$B_{32}V_{15}T_{53}^{132}$ (2)	1.02	1 : 0.4 : 1.6	LL	83 ± 8	55 ± 3
$B_{30}V_{14}T_{56}^{141}$ (2)	1.02	1 : 0.4 : 1.8	LL	85 ± 8	57 ± 3
$B_{29}V_{14}T_{57}^{145}$ (2)	1.02	1 : 0.4 : 1.8	LL	75 ± 7	n.d.
$B_{34}V_{17}T_{49}^{136}$ (3)	1.02	1 : 0.5 : 1.4	LL	86 ± 8	n.d.
$B_{16}V_{21}T_{63}^{145}$ (4)	1.02	1 : 1.2 : 3.7	CYL	55 ± 6	68 ± 4
$B_{14}V_{18}T_{68}^{165}$ (4)	1.02	1 : 1.2 : 4.6	CYL[i]	60 ± 6	72 ± 4
$B_{58}V_{27}T_{15}^{78}$ (5)	1.03	1 : 0.4 : 0.2	CYL	55 ± 6	64 ± 3
$B_{53}V_{24}T_{23}^{84}$ (5)	1.02	1 : 0.4 : 0.4	CYL	60 ± 6	65 ± 4
$B_{49}V_{23}T_{28}^{88}$(5)	1.02	1 : 0.4 : 0.5	LL	70 ± 7	n.d.

[a] Subscripts denoting the weight fraction of the corresponding block in % and the superscript the overall molecular weight in kg/mol, determined through a combination of MALDI-ToF MS and ^{1}H NMR measurements.
[b] Determined via THF-SEC, calibrated with 1,4-polybutadiene standards.
[c] Calculated according to the density of the different blocks in combination with the finally determined composition.
[d] Determined via a combination of SAXS and TEM measurements; LL lamellar morphology; CYL hexagonally packed core-shell cylinders; GYR gyroidal motif, core-shell.
[e] The error from determining the long period via TEM was estimated to be ~10%.
[f] The error resulting from the SAXS measurements (in concentrated THF solutions) depends on the width of the SAXS peak and was estimated to be ~5%.
[g] Polymers with the same number in brackets were synthesized within the same series.
[h] A non-continuous shell was observed for the polymer with the lowest P2VP content, $B_{18}V_8T_{74}^{133}$.
[i] Butadiene cylinders which exhibit a P2VP helix around the core were found to be hexagonally arranged in a P*t*BMA matrix.

Ultrathin (30–80 nm) samples for transmission electron microscopy (TEM) were cut from the as-cast polymer films with a Reichert-Jung Ultracut E equipped with a diamond knife. For polymer samples with a higher polybutadiene content than 30 wt.%, microtome cutting was performed at temperatures below the glass transition of PB (−16 °C). TEM micrographs were taken on either a Zeiss CEM 902 operating at 80 kV or a Zeiss 922 OMEGA operating at 200 kV, both in the bright field mode. In order to selectively enhance the electron density in one of the three compartments and therefore improve the contrast the samples were stained with either OsO_4 or iodine. The latter preferentially reacts with poly(2-vinylpyridine) [14], forming a charge–transfer complex while OsO_4 attacks the polybutadiene segments [27]. In both cases the P*t*BMA domains are not supposed to be affected. The methacrylic compound though is deteriorated through the electron beam and therefore considerable volume shrinkage of the respective microphase domain during the TEM measurement can lead to erroneous values [32]. The electron densities calculated for the three different compartments are as follows: ρ_e(PB) = 0.53 mol/cm^3 [33]; ρ_e(P2VP) = 0.611 mol/cm^3 and ρ_e(P*t*BMA) = 0.561 mol/cm^3 [22].

2.5. Small-angle X-ray scattering (SAXS)

Small-Angle X-Ray Scattering (SAXS) measurements were performed on the ID2 beamline at the European Synchrotron Radiation Facility (ESRF, Grenoble, France). The typical photon flux obtained at the ID2 sample position is 8×10^{12} photons/s, the energy bandwidth is $\Delta E/E = 2 \times 10^{-4}$. All experiments were obtained at 12.5 keV corresponding to an X-ray wavelength of 0.1 nm. The scattering intensities were detected by a CCD camera. The detector system is housed in a 10 m evacuated flight tube. The scattering patterns were corrected for the beam stop, the background, the used cuvettes, and the solvent prior to evaluations. In general, d-spacings obtained from concentrated solutions in THF were by around 20% larger as compared to bulk samples.

2.6. Size exclusion chromatography (SEC)

Size exclusion chromatography (SEC) with THF as eluent was performed on an apparatus equipped with PSS SDVgel columns (30 × 8 mm, 5 μm particle size) with 10^2, 10^3, 10^4 and 10^5 Å pore sizes using RI and UV detection (λ = 254 nm) at a flow rate of 1.0 mL/min (T = 40 °C). The calibration was based on 1,4-polybutadiene standards.

2.7. MALDI-ToF mass spectrometry

The number-average molecular weight of the polybutadiene precursors in each case were determined by MALDI-ToF MS on a Bruker Reflex III equipped with a 337 nm N_2 laser in the linear mode and 20 kV acceleration voltage. Sodium trifluoroacetate (NaTFA, Fluka, 99.5%) was used as salt for ion formation. *Trans*-2-[3-(4-*tert*-Butylphenyl)-2-methyl-2-propenylidene]malononitrile (DCTB) was used as matrix.

2.8. Nuclear magnetic resonance spectroscopy

^{1}H NMR measurements were performed on a 250 MHz Bruker AC spectrometer using $CDCl_3$ or THF-d_8 as solvent and tetramethylsilane (TMS) as internal standard. The molecular weights of the P2VP and the P*t*BMA block were calculated from the number-average molecular weight of the precursor obtained by MALDI-ToF mass spectrometry and the ratio of characteristic NMR signals. The molecular characteristics of the BVT triblock terpolymers are summarized in Table 1.

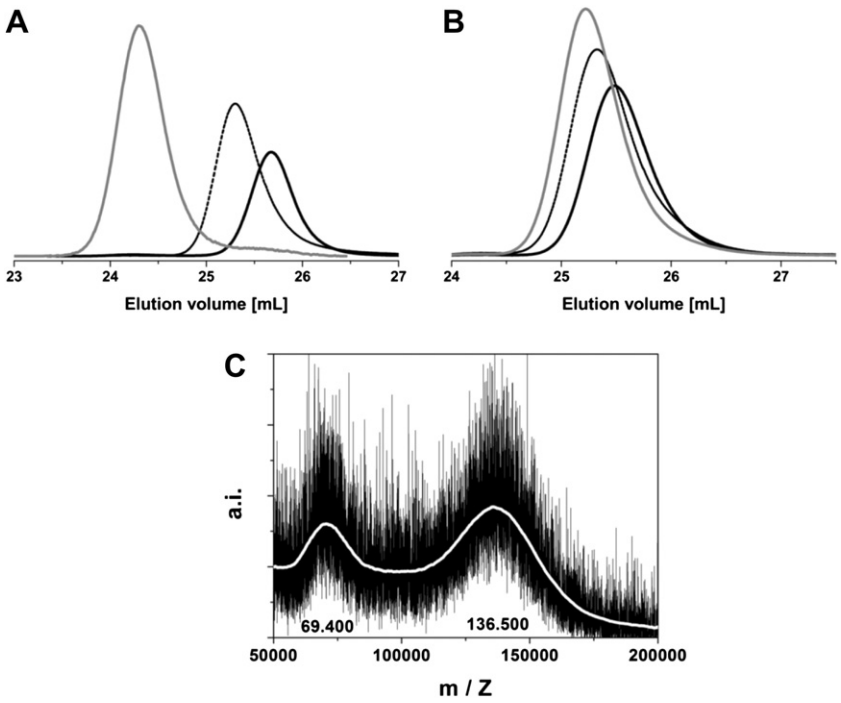

Fig. 1. THF-SEC elution traces for B^{46} (solid black line), $B_{66}V_{34}^{69}$ (dashed black line) and $B_{34}V_{17}T_{49}^{136}$ (solid grey line) (A); THF-SEC elution traces for $B_{58}V_{27}T_{15}^{78}$ (solid black line), $B_{53}V_{24}T_{23}^{84}$ (dashed black line), and $B_{49}V_{23}T_{28}^{88}$ (solid grey line) (B); MALDI-ToF mass spectrum of $B_{34}V_{17}T_{49}^{136}$, the grey line is a smoothened curve and a guide to the eye, the peak at m/z = 69.400 corresponds to doubly charged molecules.

2.9. Dynamic light scattering (DLS)

Dynamic light scattering (DLS) measurements were performed in sealed cylindrical scattering cells (d = 10 mm) at a scattering angle of 90° on an ALV DLS/SLS-SP 5022F equipment consisting of an ALV-SP 125 laser goniometer with an ALV 5000/E correlator and a He–Ne laser with the wavelength λ = 632.8 nm. The CONTIN algorithm was applied to analyze the obtained correlation functions. Apparent hydrodynamic radii were calculated according to the Stokes–Einstein equation.

2.10. Ultrasound sonication treatment

Ultrasound sonication treatment was performed in solution in small glass vials. The used instrument was a Branson Digital Sonifier equipped with a tungsten tip. Amplitude was kept at 20% and typical sonication times were 1 s followed by a break of 4 s. Total sonication times are always the summarized seconds of real sonication without breaks. Samples were always water cooled during the sonication procedure.

3. Results and discussion

3.1. Synthesis and molecular characterization of the block terpolymers

All polymers were synthesized via sequential anionic polymerization in THF in the presence of alkoxides and exhibited very low molecular weight distributions. Some exemplarily THF-SEC traces for $B_{34}V_{17}T_{49}^{136}$ including the precursors and the series of $B_{58}V_{27}T_{15}^{78}$, $B_{53}V_{24}T_{23}^{84}$, and $B_{49}V_{23}T_{28}^{88}$ are shown in Fig. 1. All obtained elution traces are monomodal. Furthermore, Fig. 1C displays a MALDI-ToF MS spectrum of $B_{34}V_{17}T_{49}^{136}$.

Two populations are observed in the MALDI-ToF mass spectrum. The main peak with m/z = 136.500 g/mol is the block terpolymer, the second at m/z = 69.400 g/mol doubly charged molecules. Please note that mass spectrometry of block copolymers, especially at molecular weights exceeding 100.000 g/mol, is a challenging task [34]. Double ionization most probably occurs due to the ionizable middle block, P2VP.

3.2. Structural characterization

The following chapter summarizes the results obtained for the microphase-separated bulk morphologies of the synthesized BVT block terpolymers by slow casting from THF solutions. For most samples, either lamellae or hexagonally arranged core-shell cylinders could be identified (Table 1), only $B_{44}V_{20}T_{36}^{98}$ showed coexisting lamellae and gyroidal parts. This composition in combination with examples for lamellae, $B_{30}V_{14}T_{56}^{141}$, and hexagonally arranged helical cylinders, $B_{14}V_{18}T_{68}^{165}$ with B core, V helix winding around the cylindrical core, and T matrix or $B_{53}V_{24}T_{23}^{84}$ with T core, V shell, and B matrix, are discussed here in more detail. Furthermore, the block terpolymer with the lowest content of P2VP, $B_{18}V_{8}T_{74}^{133}$, is forming a discontinuous shell of P2VP around the PB core in the bulk state, rendering it interesting for the generation of multicompartment polymeric nanoparticles. For $B_{18}V_{8}T_{74}^{133}$ and $B_{14}V_{18}T_{68}^{165}$, also the aggregates present in solution after crosslinking of the as-cast bulk films and subsequent sonication-assisted dissolution are investigated and shown in detail. The rest of the synthesized block terpolymers mentioned in Table 1 appears only to present a complete view. It is noteworthy that $B_{44}V_{20}T_{36}^{98}$ and $B_{30}V_{14}T_{56}^{141}$ are from the same polymer series and in an analogous way, $B_{16}V_{21}T_{63}^{145}$ and $B_{14}V_{18}T_{68}^{165}$ originate from another series as indicated by the numbers in brackets (cf. Table 1).

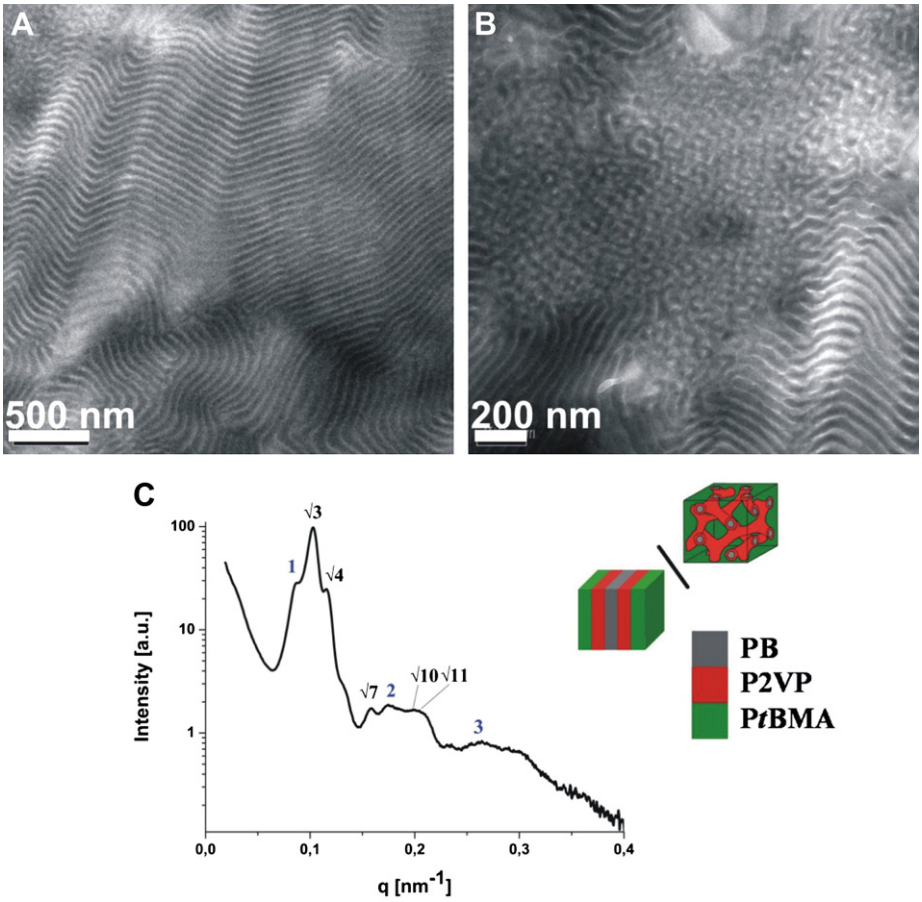

Fig. 2. TEM micrographs of $B_{44}V_{20}T_{36}^{98}$ cast from THF after staining with OsO_4 (A, B); the black part corresponds to polybutadiene; SAXS pattern of $B_{44}V_{20}T_{36}^{98}$ at 35 wt.% in THF (C), the inset shows the proposed bulk morphology.

3.3. $B_{44}V_{20}T_{36}^{98}$: coexistence of lamellae/gyroid

According to TEM, $B_{44}V_{20}T_{36}^{98}$ shows a coexistence of two morphologies (Fig. 2). Most parts of the sample show lamellae, as depicted in Fig. 2A. A partial gyroidal structure is shown in Fig. 2B. In both cases, the dark phase corresponds to the polybutadiene compartment due to OsO_4.

Fig. 2A illustrates the lamellar structure. In the upper left corner of the same TEM micrograph the transition from the lamellar into the gyroid structure is visible. A comparable location is enlarged in Fig. 2B. In Fig. 2C the corresponding SAXS pattern in THF (35 wt.%) is shown. It is rather complex and seems to contain reflexes of at least two different structural motifs. The peaks with the relative positions 1 : 2 : 3 (indicated in blue in Fig. 2C) are typical for a lamellar structure (reflections [001]; [002]; [003]). Besides, the reflexes with the relative positions $\sqrt{3} : \sqrt{4} : \sqrt{7} : \sqrt{10} : \sqrt{11}$ could be assigned to a gyroidal motif assuming that the peak at the relative position of $\sqrt{3}$ corresponds to the [211] reflection. This is in accordance with the literature [35,36]. The long period for the lamellar structure can be calculated to $d_{LAM} = 74 \pm 4$ nm (Eq. (1)). Through the assignment of the [211] reflection one can deduce the lattice pattern parameter for the gyroidal structure, $d_{GYR} = 106 \pm 5$ nm (Eq. (2)).

$$d_{LAM} = \frac{2n\pi}{q_n} \quad (1)$$

$$d_{GYR} = \frac{2\pi\sqrt{x}}{q_n} \quad (2)$$

With n being the peak order ($n = 1$ for the first peak of the lamellar pattern), q_n being the peak value obtained from the SAXS measurement (0.085 nm^{-1} for [100] and 0.102 nm^{-1} for [211]), and x the order of the peak from the gyroid pattern, in this case $x = 3$ due to $hkl =$ [211]. The interpretation of SAXS patterns from ABC triblock terpolymers bears much more complexity than for simple AB diblock copolymers. Here, the relative electron densities affect both scattering contrast and the relative scattering intensities, producing SAXS patterns where certain reflexes can be nearly extinguished [37]. Hence, the pattern shown in Fig. 2C for $B_{44}V_{20}T_{36}^{98}$ may not exhibit all the relevant reflexes necessary for a complete assignment of a gyroidal motif. Unfortunately, the signal to noise ratio in Fig. 2C strongly diminishes at $q > 0.3$ nm^{-1}, making it difficult to assign any further peaks. According to the volume/weight fractions of the three building blocks, we assume a poly(2-vinylpyridine) core with a poly(*tert*-butyl methacrylate) shell for the gyroidal motif embedded in a polybutadiene matrix.

3.4. $B_{30}V_{14}T_{56}^{141}$: lamellae

An increase of the P*t*BMA volume fraction within this terpolymer series to $\Phi_B : \Phi_V : \Phi_T = 1 : 0.4 : 1.8$ leads to a complete lamellae formation in the bulk. This is illustrated in Fig. 3. The TEM micrograph (Fig. 3A) depicts uniformly aligned lamellae in a micron sized range. The dark part (central lamella) in Fig. 3B corresponds to the polybutadiene compartment, stained with OsO_4 and flanked by smaller grey poly(2-vinylpyridine) microdomains on each side. The light parts represent the poly(*tert*-butyl methacrylate). As

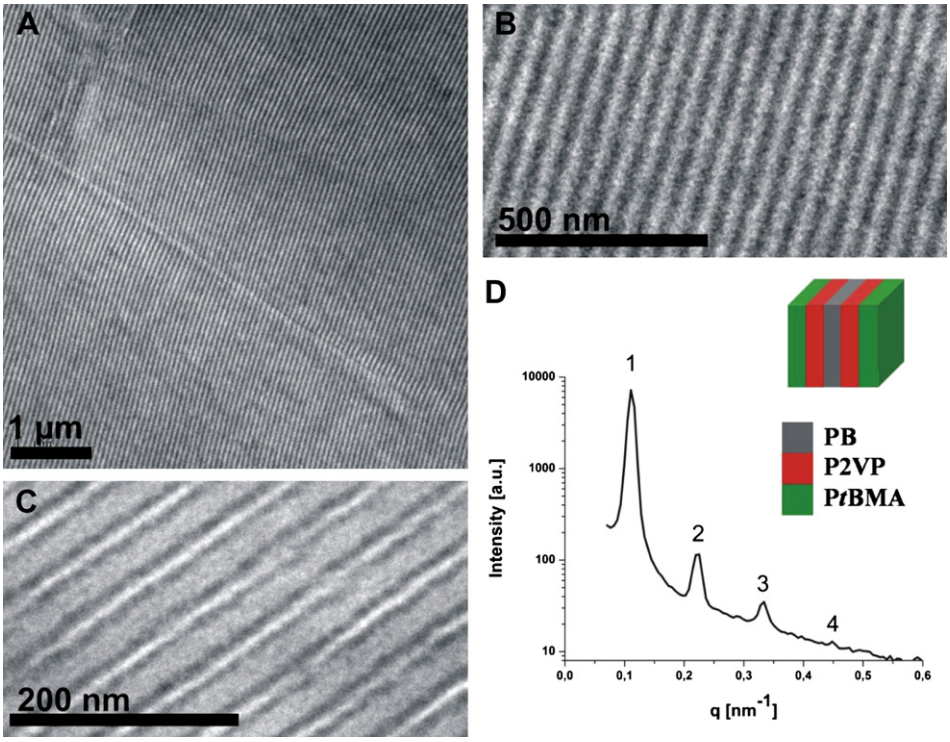

Fig. 3. TEM micrographs of $B_{30}V_{14}T_{56}^{141}$ cast from THF after staining with OsO_4 (A, B); the black phase resembles polybutadiene; after staining with iodine, the dark parts resemble P2VP (C), scale bar corresponds to 200 nm; SAXS pattern of $B_{30}V_{14}T_{56}^{141}$ at 35 wt.% in THF (C), the inset shows the proposed bulk morphology.

mentioned earlier, the microdomain dimensions from TEM do not necessarily coincide with the calculated volume fractions, caused by the electron beam damage of the methacrylic phase. Hence, the P*t*BMA domains are not significantly larger than the PB compartments, although the volume fraction is almost the double. It has been reported that methacrylic domains may shrink to less than half of the expected value in that way [38].

Fig. 3C shows a TEM micrograph after staining with iodine. Here, the dark domains correspond to P2VP. The ll morphology can be nicely seen. Two parallel dark P2VP domains are adjacent to a lighter PB lamella. The lightest parts again are P*t*BMA, which is not affected by the staining procedure. The long periods obtained from TEM are around 60 nm in both cases. In Fig. 3D the SAXS pattern in solution (35 wt.% in THF) is depicted. The lamellar morphology is again confirmed and the characteristic peaks for such structural motifs at integer multiples of the first order peak are visible. The relative reflex positions 1 : 2 : 3 : 4 are related to the [100] : [200] : [300] : [400] reflections. From the SAXS measurements, the long period was calculated to $d_{LAM} = 57 \pm 3$ nm (with $q_n = 0.111$ nm^{-1} for [100]) and is in good agreement with the results obtained from TEM ($d_{LAM,\ TEM} = 85 \pm 8$ nm), considering the shear forces during the microtome cutting. Apart from the bulk properties, $B_{30}V_{14}T_{56}^{141}$ was shown to form a multitude of different multi-compartmental structures in solution, depending on the preparation conditions [39,40].

3.5. $B_{18}V_8T_{74}^{133}$: core-shell cylinders with a discontinuous shell

The terpolymer with the lowest content of P2VP, 8%, exhibits a core-shell cylindrical morphology. The hexagonal arrangement, although slightly distorted, is shown in Fig. 4A, the corresponding FFT pattern in the inset, Fig. 4B. In the enlargement, Fig. 4C, it can be seen that the cylinders are slightly ill-shaped. In our opinion, the low content of P2VP results in the formation of a non-continuous shell around the PB core. This then results in the generation of an additional interface between PB and P*t*BMA, although, according to the block sequence, these compartments are not directly linked. In Fig. 4D the microtome cut has been stained with iodine, enhancing the electron density in the P2VP phase. Here, the disrupted nature of the P2VP shell is more evident, as it appears darker. Several unconnected black dots are surrounding the cylindrical PB core.

The formation of an additional interface between the first and the last block of block terpolymers upon drastically reducing the volume fraction of the middle block has already been reported before [16]. If the χ-parameters for the BVT block terpolymers are compared, $\chi_{BT} = 0.007$, $\chi_{BV} = 0.13$–0.26, and $\chi_{BV} = 0.325$ [28,29], PB and P*t*BMA are supposed to show the lowest incompatibility. Moreover, PB and P2VP should avoid each other most. Therefore, it seems possible that the breaking up of an existing continuous P2VP shell reduces the interfacial tension of the whole system even though a new interface between PB and P*t*BMA is generated. Comparable bulk morphologies have also been reported for SBM block terpolymers [41]. The SAXS pattern of $B_{18}V_8T_{74}^{133}$ in THF (35 wt.%) is shown in Fig. 4E. All important reflections for hexagonally arranged cylinders are present and could be successfully assigned, [100], [110], [200], [210], [300], [220], and [310]. Calculation of the long period from the SAXS pattern results in $d_{CYL} = 67 \pm 4$ nm (Eq. (3)).

$$d_{CYL,eff} = \frac{d_{CYL}}{\sin(60^\circ)} = \frac{2}{\sqrt{3}} d_{CYL} \tag{3}$$

With d_{CYL} calculated according to Eq. (1).

$$R_{CYL} = D_{CYL,eff} \sqrt{\frac{2\Phi_{CYL}}{\sqrt{3}\prod}} \tag{4}$$

A further evaluation (Eq. (4), with Φ_{CYL} being the volume fraction of the cylinder forming phase) gives rise to the cylinder radius,

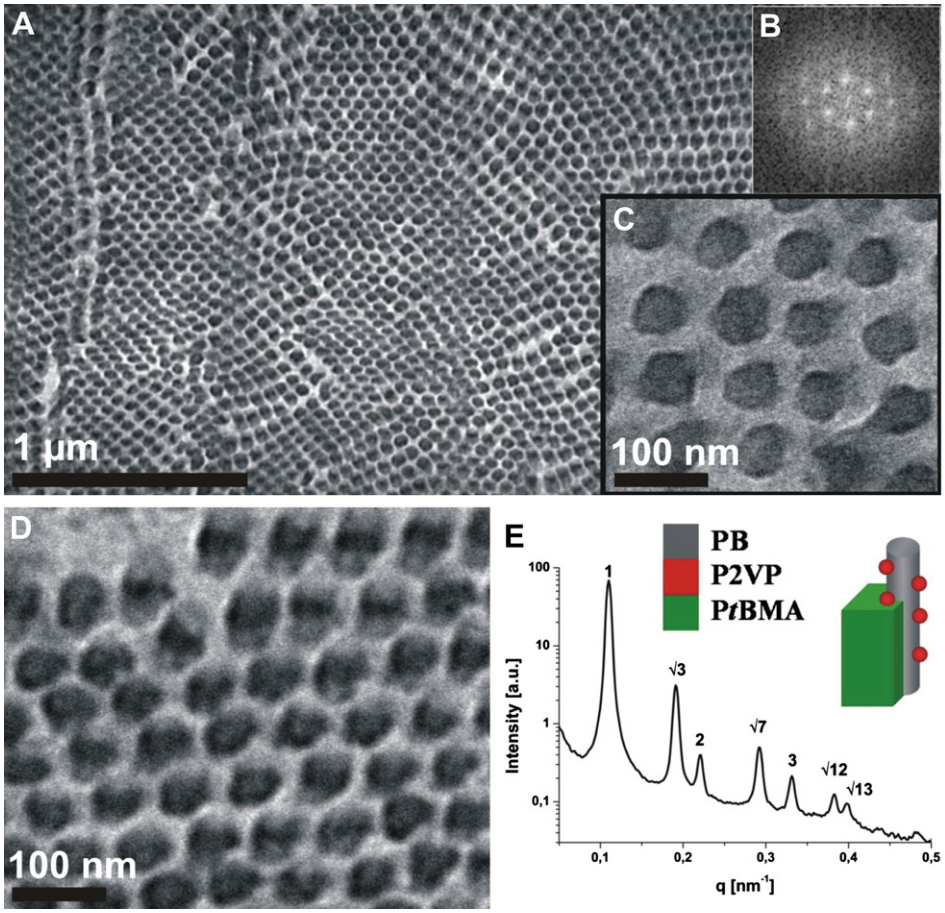

Fig. 4. TEM micrographs of $B_{18}V_8T_{74}^{133}$ cast from THF after staining with OsO_4 (A); the black phase resembles PB; the inset (B) shows an FFT pattern obtained from A; enlargement from A (C); TEM micrograph of $B_{18}V_8T_{74}^{133}$ cast from THF after staining with iodine (D), the black phase shows P2VP; SAXS pattern of $B_{18}V_8T_{74}^{133}$ at 35 wt.% in THF (E), the inset shows the proposed bulk morphology.

$R_{CYL} = 20 \pm 1$ nm. From TEM, the cylinder radius was estimated to be slightly larger, $R_{CYL} = 25 \pm 3$ nm, probably due to distortion of the structure occurring during the microtome cutting. Besides that, both TEM and SAXS confirm the formation of a hexagonally packed cylindrical structure.

To further elucidate the structure of this P2VP shell, the PB core of the cylinders was crosslinked in the bulk. Therefore, films with up to 10% UV-photoinitiator were cast from THF and exposed to UV-light for 2 h afterwards. Subsequent swelling followed by sonication of the polymer films in THF lead to dissolution of the self-assembled structures. Soxhlett extraction of the crosslinked polymer samples with THF was used to estimate the degree of crosslinking, around 75% in this case. These were then drop-coated onto carbon-coated grids and analyzed by TEM. Dynamic light scattering (DLS) was also performed to assess the average size of the particles in dependence of the sonication time. The results are shown in Fig. 5.

Fig. 5A depicts a TEM micrograph of $B_{18}V_8T_{74}^{133}$ cylinders deposited from THF solution after 10 min sonication. The cylinders are very uniform in diameter but show a rather large length distribution due to the sonication process. The diameter measured by TEM in this case is around 75 ± 7 nm, significantly larger than via calculation from d_{CYL}. This is be due to swelling of the partially crosslinked structure in THF, a good solvent for all the three blocks. The (in solution) swollen cylinders then are deposited onto the TEM grid like "pancakes", explaining the increased width. In Fig. 5B and C enlargements of the same sample are displayed. Here, the non-continuous P2VP shell is more evident. Especially in Fig. 5B, a rather random distribution of small black dots along the cylinder can be seen. We suppose that these are spherical P2VP domains located on the PB cylinder. Through the dissolution in THF, P2VP also swells and, in some cases, this than may lead to a partially continuous corona and a tubular appearance of the polymeric cylinders, as displayed in Fig. 5C, despite the low volume fraction of the middle block. Together with the results presented in Fig. 4, we propose the following bulk morphology for $B_{18}V_8T_{74}^{133}$, depicted in Fig. 5D: hexagonally arranged PB cylinders (grey) covered by P2VP spheres (red) embedded in a P*t*BMA matrix. Fig. 5E shows the DLS auto-correlation functions after different sonication times. A clear shift with increasing sonication time towards lower decay times is observable. The corresponding CONTIN plots at $\theta = 90^\circ$ for 1 (solid black line) and 10 min (solid grey line) are displayed in Fig. 5F. In the beginning, after 1 min sonication, apparent hydrodynamic radii of 65 and 310 nm are observed. After 10 min sonication this is decreasing to a single, although far broadened, peak at $<R_h>_{z,app} = 185$ nm. The broadening can be interpreted as an artifact of the DLS measurement, as the CONTIN algorithm assumes a spherical particle shape, which is not the case here.

3.6. $B_{14}V_{18}T_{68}^{165}$: P2VP helix around hexagonally arranged PB cylinders

The terpolymer with a rather high content of P*t*BMA, $\Phi_B : \Phi_V : \Phi_T = 1 : 1.2 : 4.6$, also exhibits a core-shell cylindrical morphology,

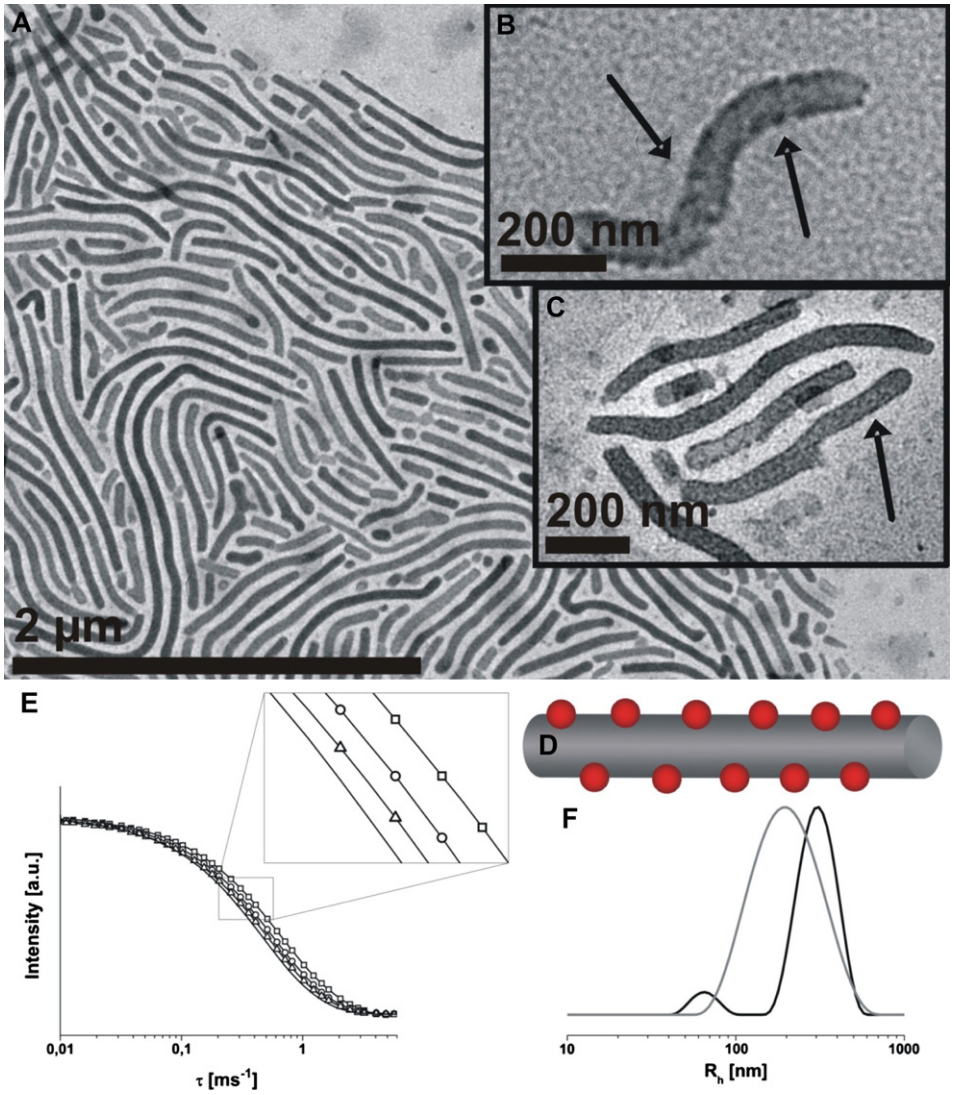

Fig. 5. TEM micrograph for $B_{18}V_8T_{74}^{133}$ after 10 min sonication and drop-coating from THF onto a TEM grid (A); enlargement of one single cylinder (B); enlargement of several cylinders after staining with iodine (C); schematic drawing of the proposed bulk structure, PB cylinder (grey) bearing P2VP spheres (red) embedded in a P*t*BMA matrix (D); DLS autocorrelation functions for $B_{18}V_8T_{74}^{133}$ after crosslinking in the bulk and subsequent sonication in THF for 1 (-□-), 3 (-○-), 5 (-Δ-), and 10 min (solid black line) (E), the inset shows a zoom of the relevant region; DLS CONTIN plots at $\theta = 90°$ for $B_{18}V_8T_{74}^{133}$ cylinders in THF after sonication for 1 (solid black line, $<R_h>_{z,\ app} = 65$ and 310 nm) and 10 min (solid grey line, $<R_h>_{z,\ app} = 185$ nm) (F). For interpretation of the references to colour in this figure legend, the reader is referred to the web version of this article.

as illustrated in Fig. 6. The dark phase represents polybutadiene, the core of the cylinders, due to the OsO_4 staining (Fig. 6A). The grey compartments correspond to the surrounding poly(2-vinylpyridine) shell and the light parts show poly(*tert*-butyl methacrylate), the matrix. As for the other BVT terpolymer morphologies discussed here, the P*t*BMA compartment suffers from considerable shrinkage caused through radiation damage. The inset, Fig. 6B, shows an FFT pattern from Fig. 6A, confirming the hexagonal arrangement of the cylinders. Fig. 6C presents an "on-top" view onto the cylinders heads, being slightly distorted. Here, the microtome cut has been stained with iodine, which enhances the electron density in the P2VP shell.

A dark-grey "horse-shoe" around each PB cylinder is observed in Fig. 6C. Surprisingly, the P2VP shell is not continuous, which would result in the formation of a complete ring around the PB compartment. In Fig. 6D a side-view of the cylinders is presented, also stained with iodine for a better visualization of the P2VP part. Clearly, the formation of a double-stranded P2VP helix can be seen. The helical pitch is around 160 nm. The finding of a non-continuous shell around the PB core and therefore the generation of an additional interface between PB and P*t*BMA can be explained as before ($B_{18}V_8T_{74}^{133}$). The difference here is that the P2VP block is somewhat longer, resulting in a higher volume fraction. Helical morphologies have been reported before for SBM block terpolymers [16,41]. Here, a morphology containing PS cylinders with a PB helix around them embedded in a PMMA matrix was observed. The inset in Fig. 6D displays the proposed bulk structure in this case, a grey PB cylinder coated with a red P2VP helix. The SAXS pattern from THF solution (35 wt.%) is shown in Fig. 6E. The scattering maxima appear at relative positions of $1 : \sqrt{3} : 2 : 3 : \sqrt{12} : \sqrt{13}$ which correspond to the [100], [110], [200], [300], [220] and [310] reflections of a cylindrical structure. The [210] peak is missing. Calculation of the long period from the SAXS pattern results in $d_{CYL} = 72 \pm 4$ nm. A further evaluation gives rise to the cylinder diameter, $R_{CYL} = 21 \pm 1$ nm (cf. Equations (3) and (4)). From TEM, the cylinder radius was estimated to be slightly larger, $R_{CYL} = 25 \pm 3$ nm.

To further elucidate the structure of these cylinders in the bulk, the PB core of the cylinders was crosslinked like shown before for

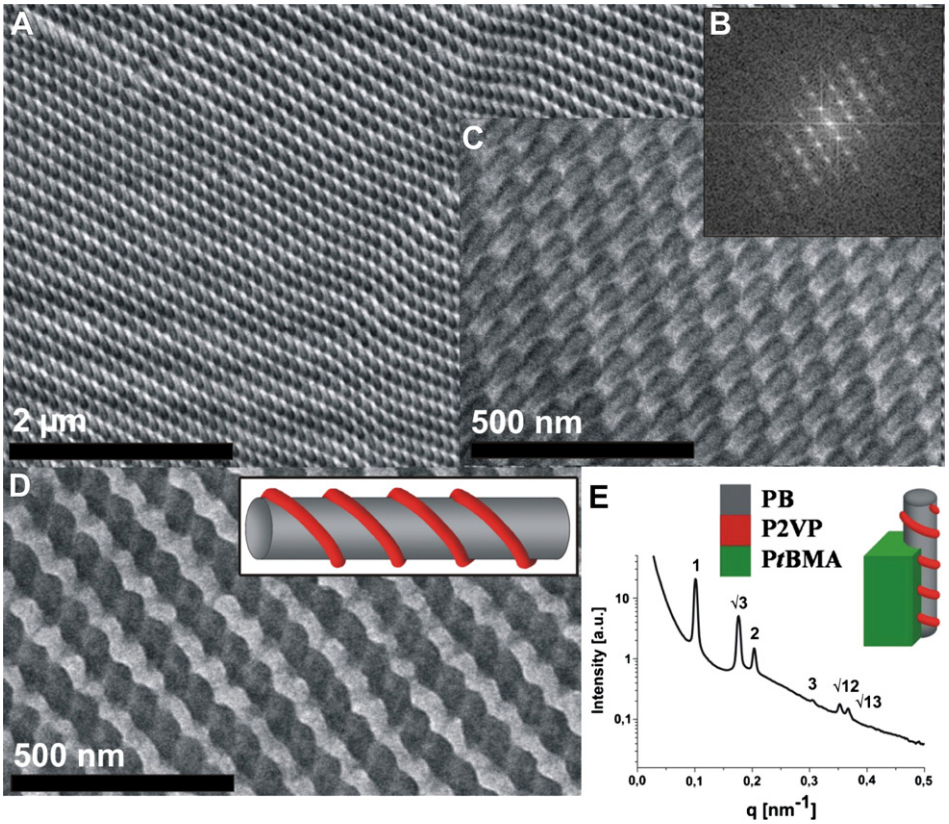

Fig. 6. TEM micrographs of $B_{14}V_{18}T_{68}^{165}$ cast from THF after staining with OsO_4 (A); the black phase resembles PB; the inset (B) shows an FFT pattern obtained from A; TEM micrograph of $B_{14}V_{18}T_{68}^{165}$ cast from THF after staining with iodine (C), the black phase shows P2VP; Side-view onto the cylinders, the inset depicts what we suppose is the bulk morphology, PB cylinders (grey) carrying a P2VP helix (red) embedded in a P*t*BMA matrix (D); SAXS pattern of $B_{14}V_{18}T_{68}^{165}$ at 35 wt.% in THF (E), the inset shows the proposed bulk morphology. For interpretation of the references to colour in this figure legend, the reader is referred to the web version of this article.

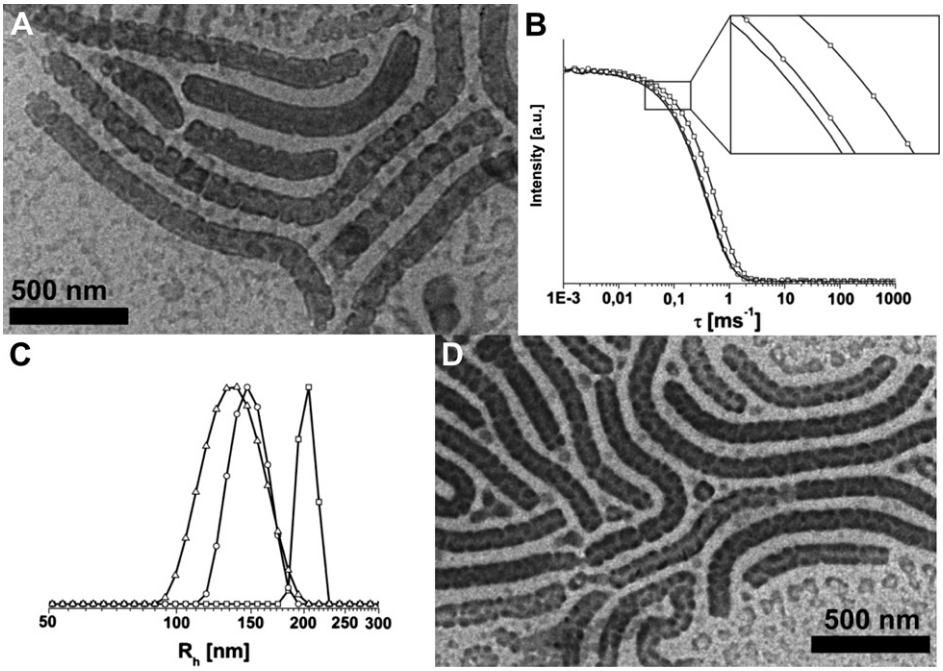

Fig. 7. TEM micrograph for $B_{14}V_{18}T_{68}^{165}$ after 5 min sonication and drop-coating onto a TEM grid (A); DLS autocorrelation functions for $B_{14}V_{18}T_{68}^{165}$ after crosslinking in the bulk and subsequent sonication in THF for 5 ((-□-)), 10 ((-○-)), and 15 min (solid black line) (B), the inset shows a zoom of the relevant region; DLS CONTIN plots at $\theta = 90^\circ$ for $B_{14}V_{18}T_{68}^{165}$ cylinders in THF after sonication for 5 ((-□-), $<R_h>_z = 205$ nm), 10 ((-○-),$<R_h>_z = 145$ nm), and 15 min (-Δ-, $<R_h>_z = 130$ nm) (C); TEM micrograph for the same sample as (A) after staining with iodine (D).

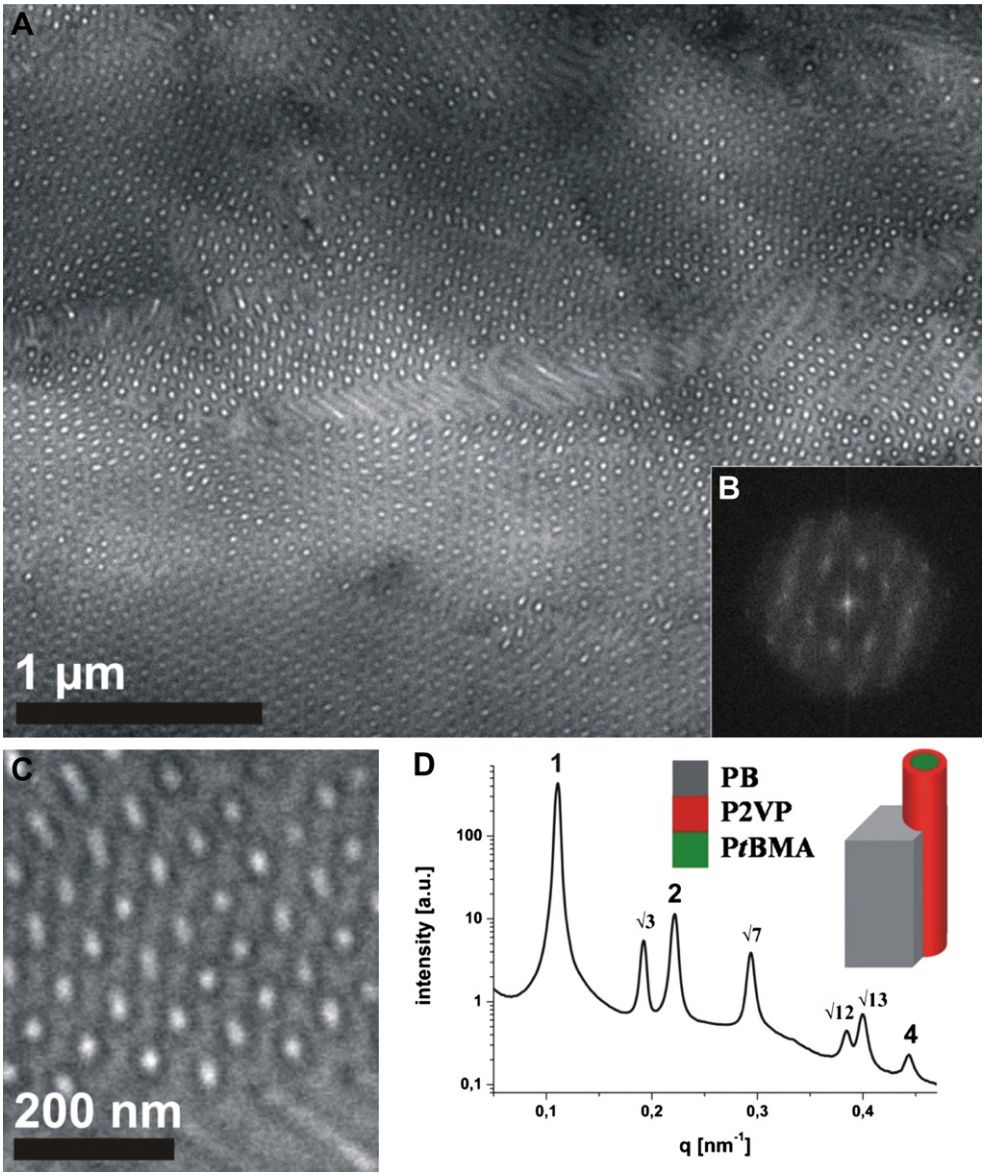

Fig. 8. TEM micrographs of $B_{58}V_{27}T_{15}^{78}$ cast from THF after staining with iodine (A, C); the black phase resembles P2VP; scale bar corresponds to 1 µm (A) and 200 nm (C); the inset (B) shows an FFT pattern obtained from A; SAXS pattern obtained from $B_{58}V_{27}T_{15}^{78}$ at 30 wt.% in THF (D), the inset shows the proposed bulk morphology.

$B_{18}V_8T_{74}^{133}$. Again, films were cast with addtional 10% UV crosslinking agent from THF and exposed to UV-light for 2 h afterwards. Fig. 7 summarizes the DLS and TEM results.

Fig. 7A shows a TEM micrograph of $B_{14}V_{18}T_{68}^{165}$ cylinders deposited from THF solution after crosslinking with 10% TPO and subsequent sonication for 5 min. Again, the cylinders are uniform in diameter but show a rather large length distribution. The helical morphology cannot be definitely confirmed, although the cylinders do not exhibit an homogeneous surface. Here, the diameter measured via TEM is around 100 nm, almost deviating by a factor of 2 from the SAXS results. This can be attributed to the swelling of the partially crosslinked cylindrical core in THF in combination with the sample preparation. Fig. 7B shows the DLS autocorrelation functions after different sonication times. The decay times shift with increasing sonication towards lower values. The corresponding CONTIN plots at $\theta = 90^\circ$ for 5 ((-□-)), 10 ((-○-)), and 15 min (-Δ-) are displayed in Fig. 7C. After 5 min sonication a value for $<R_h>_{z,\,app}$ of 205 nm was obtained. Surprisingly, the population shows a quite narrow distribution ($PDI_{DLS} = 0.08$). After 10 min sonication, $<R_h>_{z,\,app} = 145$ nm, and after 15 min $<R_h>_{z,\,app} = 130$ nm were measured. Again, the DLS plots show a broadening with increasing sonication time, attributed as an artifact of the CONTIN algorithm.

Fig. 7D shows basically the same sample like Fig. 7A after staining with iodine. Dark, round spots with a diameter of approximately 15–20 nm are present on the PB core of the cylinders, representing the P2VP compartments. Apparently, upon contact with THF, a good solvent for P2VP, the helices swell and upon deposition of the cylinders onto the TEM grid the polymer chains collapse again into spherical domains. Nevertheless, these cylindrical nanoparticles could serve as interesting multi-compartmental templates for the generation of hybrid structures. The characterization of these compartmentalized cylindrical micelles in solution will be the subject of a forthcoming publication [42].

3.7. $B_{58}V_{27}T_{15}^{78}$: inverted core-shell cylinders

The previously discussed terpolymer, $B_{14}V_{18}T_{68}^{165}$, was also tested as a precursor for the fabrication of thin-film composite

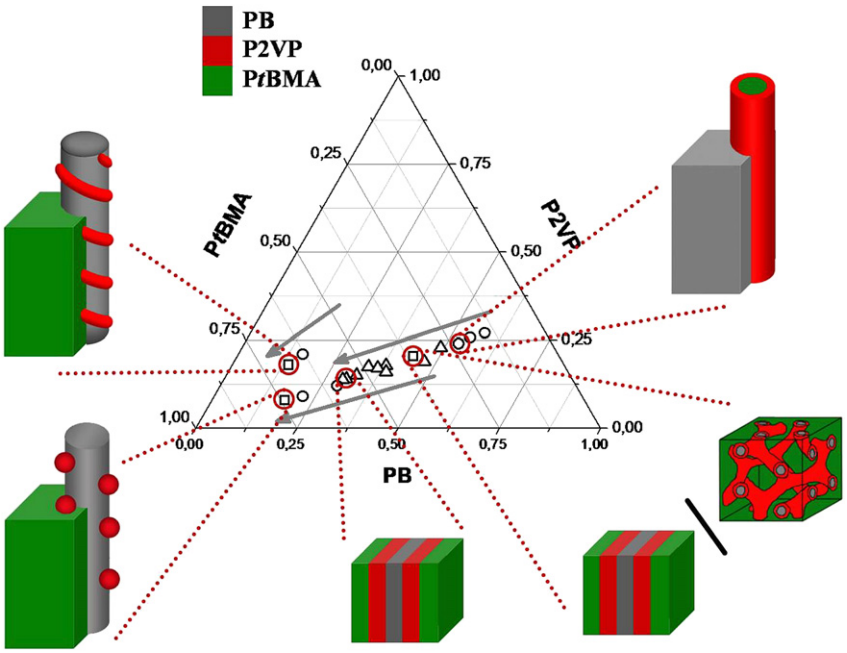

Fig. 9. Ternary phase diagram obtained for several series of BVT block terpolymers, the grey phase resembles polybutadiene, the red phase poly(2-vinylpyridine), and the green phase poly(*tert*-butyl methacrylate); morphologies are lamellar (△), cylindrical (○), or either mixtures or unusual structures (spheres on cylinders or helices on cylinders). For interpretation of the references to colour in this figure legend, the reader is referred to the web version of this article.

membranes [24]. Well ordered arrays of core-shell cylinders aligned perpendicular to the surface on various substrates could be produced. However, the removal of the polybutadiene core of these thin-film structures to generate porous structures is not so straightforward. It is therefore of interest to invert the structure, resulting in a polybutadiene matrix with embedded cylinders consisting of a P*t*BMA core and a P2VP shell. The genuine advantage would be that the cylinder cores could be easily removed through UV-induced depolymerization of the P*t*BMA, giving access to porous materials with pH-responsive (P2VP) pore walls. Thus, a polymer series with volume fractions $\Phi_B : \Phi_V : \Phi_T = 1 : 0.4 : 0.2–0.5$ was synthesized. As mentioned in Table 1, both $B_{58}V_{27}T_{15}^{78}$ and $B_{53}V_{24}T_{23}^{84}$ show hexagonally packed cylinders with a P*t*BMA core although only $B_{58}V_{27}T_{15}^{78}$ is discussed here in more detail. TEM images for this block terpolymer cast from THF and stained with iodine as well as SAXS data are shown in Fig. 8.

In Fig. 8A an "on-top" view onto the cylinders is shown. Clearly, a hexagonal pattern can be observed. This is highlighted in the FFT in Fig. 8B. Fig. 8C displays an enlargement where the cylinder fine structure can be seen. The light core of the cylinders is P*t*BMA, already deteriorated through the incident electron beam. The dark ring resembles the P2VP shell, darkened through the staining treatment with iodine, surrounded by the grey PB matrix. If measured by TEM, the long period for this hexagonally packed morphology is 55 ± 6 nm and the average cylinder diameter is 40 nm (20 nm for the P*t*BMA core and 2 × 10 nm for the P2VP shell). It is apparent that the as-cut films are rather strongly bended and distorted as a result of the high polybutadiene content. Microtome cutting had to be performed at low temperatures (−30 °C) to reduce the softness of the material. The SAXS pattern from THF solution (30 wt.%) is shown in Fig. 8D. The scattering maxima appear at relative positions of $1 : \sqrt{3} : 2 : \sqrt{7} : \sqrt{12} : \sqrt{13} : 4$ which correspond to the [100], [110], [200], [210], [220], [310] and [400] reflections of a hexagonal cylindrical structure. Calculation of the long period from the SAXS pattern results in $d_{CYL} = 64 \pm 3$ nm (Eq. (3)) and is in good agreement with the values obtained via TEM measurements.

4. Phase diagram for BVT block terpolymers

The results from the previous chapters are summarized in a ternary phase diagram (Fig. 9). The terpolymers discussed within the scope of this manuscript are highlighted (red circles) and their proposed bulk morphologies are schematically depicted around the phase diagram. Within each polymer series the grey arrow indicates an increasing volume fraction of P*t*BMA.

Open spheres resemble cylindrical morphologies, open triangles lamellar structures. All non-typical examples are represented by open rectangles: the helical morphology for $B_{14}V_{18}T_{68}^{165}$, the cylinders with a non-continuous shell for $B_{18}V_8T_{74}^{133}$, and the coexisting between lamellae and gyroid for $B_{44}V_{20}T_{36}^{98}$. In Table 1 the different block terpolymers of one series are marked by the numbers in brackets. Within series 1, the morphology changes from LL for $B_{47}V_{19}T_{34}^{61}$ and $B_{38}V_{16}T_{46}^{82}$ to hexagonally arranged core-shell cylinders, PB core and P2VP shell for $B_{29}V_{12}T_{59}^{86}$, $B_{22}V_9T_{69}^{109}$, and $B_{18}V_8T_{74}^{133}$. The content of P2VP for $B_{29}V_{12}T_{59}^{86}$ and $B_{22}V_9T_{69}^{109}$ is still high enough to form a continuous shell. For $B_{18}V_8T_{74}^{133}$, this is not the case. The lowest content of P2VP, 8 wt.%, results in the formation of spherical domains situated on the PB core of the cylinder. For series 2, the high butadiene content of $B_{55}V_{26}T_{19}^{77}$ leads to the formation of P*t*BMA cylinders with a P2VP shell in a PB matrix. With increasing P*t*BMA content, a mixed volume structure consisting of lamellae and a gyroidal motif was found for $B_{44}V_{20}T_{36}^{98}$. Higher volume fractions of P*t*BMA resulted in the formation of purely lamellar morphologies for $B_{38}V_{18}T_{44}^{112}$, $B_{37}V_{17}T_{46}^{117}$, $B_{32}V_{15}T_{53}^{132}$, $B_{30}V_{14}T_{56}^{141}$, and $B_{29}V_{14}T_{57}^{145}$. Same accounts for the only block terpolymer of series 3, $B_{34}V_{17}T_{49}^{136}$. For series 4, hexagonally arranged core-shell cylinders with a PB core and a P2VP shell are obtained for $B_{16}V_{21}T_{63}^{145}$. The cylindrical arrangement of the PB segments is also present in the case of $B_{14}V_{18}T_{68}^{165}$ although here the middle block forms a helix along the PB cylinders. For the last series, 5, inverted core-shell cylinders with a P*t*BMA core and a P2VP shell are obtained for $B_{58}V_{27}T_{15}^{78}$ and $B_{53}V_{24}T_{23}^{84}$. Upon further increasing the P*t*BMA volume fraction, a lamellar morphology is found for $B_{49}V_{23}T_{28}^{88}$.

5. Conclusion

Several series of polybutadiene-*block*-poly(2-vinylpyridine)-*block*-poly(*tert*-butylmethacrylate) (BVT) block terpolymers have been synthesized and exhaustively characterized. Among the morphologies obtained are lamellar (LL), cylindrical (CYL), a mixture of gyroidal and lamellar (GYR/LL), and cylindrical morphologies with a non-continuous P2VP shell (spheres on cylinders for $B_{18}V_8T_{74}^{133}$ and helices on cylinders for $B_{14}V_{18}T_{68}^{165}$). Especially the latter two block terpolymers were shown to be very interesting precursors for the generation of novel multi-compartmental core-crosslinked cylindrical polymeric nanoparticles. For this, a sonication-assisted pathway developed in our group has been adopted and it could be demonstrated that the size of the generated nanoparticles can be tuned by the sonication time in a fashionable way. The results presented here in combination with earlier work nicely show that the BVT system provides a suitable platform for the preparation of advanced and sophisticated nanostructured systems in the bulk, in solution, and in thin films.

Acknowledgements

Financial support was received from the Volkswagen Foundation in the framework of the “Complex Materials” programme. The authors would like to thank Dr. Holger Schmalz and Denise Danz for help during the synthesis of the polymers and for MALDI-ToF measurements. Dr. Kristin Schmidt is acknowledged for SAXS measurements on beamline ID2 in Grenoble. We thank Dr. Markus Drechsler for some TEM measurements and Katharina and Benjamin Schatz for help with the illustrations. We also thank Sabine Wunder for performing SEC measurements. The crosslinking agent, Lucirin-TPO®, was kindly provided by BASF.

References

[1] Lazzari M, Lopez-Quintela MA. Adv Mater 2003;15:1583.
[2] Hadjichristides N, Pispas S. Adv Polym Sci 2006;200:37–55.
[3] Hillmyer MA. Adv Polym Sci 2005;189:137–81.
[4] Li H, Huck WTS. Curr Opin Solid State Mater Sci 2002;6:3.
[5] Ishizu K, Tsubaki K, Mori A, Uchida S. Prog Polym Sci 2003;28:27.
[6] Francis R, Lepoittevin B, Taton D, Gnanou Y. Macromolecules 2002;35:9001.
[7] Klok H-A, Lecommmandoux S. Adv Mater 2001;13(16):1217–29.
[8] Liu G, Ding J, Hashimoto T, Kimishima K, Winnik FW, Nigam S. Chem Mater 1999;11(8):2233–40.
[9] Liu G, Ding J, Stewart S. Angew Chem Int Ed 1999;38:835.
[10] Abetz V, Simon PFW. Adv Polym Sci 2005;189:125–212.
[11] Hadjichristidis N, Iatrou H, Pitsikalis M, Pispas S, Avgeropoulos A. Prog Polym Sci 2005;30:725–82.
[12] Jung K, Abetz V, Stadler R. Macromolecules 1996;29:1076.
[13] Stadler R, Auschra C, Beckmann J, Krappe U, Voigt-Martin I, Leibler L. Macromolecules 1995;28:3080.
[14] Hückstädt H, Göpfert A, Abetz V. Macromol Chem Phys 2000;201:296.
[15] Hückstädt H, Göpfert A, Abetz V. Polymer 2000;41:9089–94.
[16] Krappe U, Stadler R, Voigt-martin I. Macromolecules 1995;28:4558–61.
[17] Breiner U, Krappe U, Thomas EL, Stadler R. Macromolecules 1998;31(1):135–41.
[18] Brinkmann S, Stadler R, Thomas EL. Macromolecules 1998;31:6566.
[19] Liu Y, Abetz V, Müller AHE. Macromolecules 2003;36:7894–8.
[20] Erhardt R, Böker A, Zettl H, Kaya H, Pyckhout-Hintzen W, Krausch G, et al. Macromolecules 2001;34:1069–75.
[21] Walther A, Andre X, Drechsler M, Abetz V, Müller AHE. J Am Chem Soc 2007;129(19):6187–98.
[22] Ludwigs S, Böker A, Abetz V, Müller AHE, Krausch G. Polymer 2003;44:6815–23.
[23] Ludwigs S, Böker A, Voronov A, Rehse N, Magerle R, Krausch G. Nat Mater 2003;2:744–7.
[24] Sperschneider A, Schacher F, Gawenda M, Tsarkova L, Müller AHE, Ulbricht M, et al. Small 2007;3:1056–63.
[25] Sperschneider A, Schacher F, Tsarkova L, Müller AHE. submitted for publication.
[26] Barton AF. CRC handbook of polymer liquid interaction parameters and solubility parameters. Boca Raton: CRC Press; 1990.
[27] Kato KJ. Polym Sci Polym Lett 1966;4:35.
[28] Mark JE. Physical properties of polymers handbook. Woodbury: American Institute of Physics Press; 1996.
[29] Schubert DW, Stamm M, Müller AHE. Polym Eng Sci 1999;39:1501.
[30] Giebeler E, Stadler R. Macromol Chem Phys 1997;198(12):3815–25.
[31] Freyss D, Rempp P, Benoît H. Polym Lett 1964;2:217.
[32] Sawyer LC, Grubb DT. Polymer microscopy. London: Chapman & Hall; 1996.
[33] Goldacker T. Bayreuth: Dissertation 1999.
[34] Montaudo G, Samperi F, Montaudo MS. Prog Polym Sci 2006;31(3):277–357.
[35] Matsen MW. J Chem Phys 1998;108(2):785–96.
[36] Garstecki P, Holyst R. Phys Rev E 2001;64(2):021501.
[37] Mogi Y, Nomura M, Kotsuji H, Ohnishi K, Matsushita Y, Noda I. Macromolecules 1994;27:6755–60.
[38] Abetz V, Goldacker T. Macromol Rapid Comm 2000;21:16–34.
[39] Schacher F, Walther A, Müller AHE. Langmuir 2009;25:10962–9.
[40] Schacher F, Walther A, Ruppel M, Drechsler M, Müller AHE. Macromolecules 2009;42:3540–8.
[41] Breiner U, Krappe U, Abetz V, Stadler R. Macromol Chem Phys 1997;198:1051.
[42] Schacher F, Rudolph T, Drechsler M, and Müller AHE. Manuscript in preparation.